

Current progress in vanadium oxide nanostructures and its composites as supercapacitor electrodes

Raktima Basu,* Sandip Dhara*

Surface and Nanoscience Division, Indira Gandhi Centre for Atomic Research, Homi Bhabha

National Institute, Kalpakkam-603102, India

Email: raktimabasu14@gmail.com; dhara@igcar.gov.in

Abstract

In recent years, vanadium oxides have gained immense attention in the field of energy storage devices due to their low-cost, layered structure and multi-valency despite their limited electrical conductivity and lower structural stability. In this brief review, we have tried to focus on electrochemical properties of the stoichiometric vanadium oxides along with VO_x composites. The morphology engineering, doping with heteroatom and formation of composites with carbon-based materials and/or conducting polymers in enhancing the supercapacitive performances of the vanadium oxides are discussed in details. Finally, the potentiality and challenges of vanadium oxides nanocomposites for supercapacitor applications are discussed.

Keywords: supercapacitor, vanadium oxide, specific capacitance, pseudocapacitance, phase transition

1. Introduction:

In recent time, supercapacitors (SCs) are one of the emerging technologies used for clean energy prospect. The higher power density, low specific energy, longer cycle life, and environmental affability made the SCs superior compared to conventional batteries. However, the scientific community is working towards increasing the specific energy of SCs by finding a suitable electrode material. Carbon materials, conducting polymers, and metal oxide or hydroxides are reported to be suitable candidates as electrodes for SC [1-3]. Carbon materials such as activated carbon, carbon nanotube and graphene provide excellent electrical conductivity and chemical stability [4], however, they come with narrow charge storage capacity and relatively low energy density [1]. On the other hand, the conducting polymers are a good choice as a pseudocapacitor [3]. Nevertheless, the electrochemical stability is poor. Towards this end, transition metal oxides (TMOs) are alternative candidates due to their multiple oxidation states and rapid redox kinetics [2]. Amongst other TMOs [5-7], vanadium oxides have received recent attention owing to their low-cost, variety of valence states, and abundant sources [8-10]. V is a transition metal ($[\text{Ar}]3d^34s^2$) with valences in the range of +2 to +5 with major oxides as VO, V_2O_3 , VO_2 , and V_2O_5 [11]. However, the V-O phase diagram comprises mixed-valence oxides comprehending two oxidation states, e.g. V_4O_9 , V_6O_{13} , V_8O_{15} , V_7O_{13} , V_6O_{11} , among others which permit conversion between oxides of different stoichiometry easily and make it unstable during charging- discharging cycle. As the composition, oxidization state, and structural phase of a material have a significant role on electrochemical properties; the exchange of valency along with structural instability for these materials results in poor electrochemical and cycle performance. Issues related to the presence of multiple valence states of V [10], as well as its stability affecting retention of capacitance and its efficiency, are found to hinder further utility in SCs. The poor charge storage properties and electrical conductivity of vanadium oxides are reported to be succeeded by

fabricating directly on the current collector, doping element, or by nanostructure engineering. There are several reports on SC properties of VO_x composites as well as individual vanadium oxides such as VO₂, V₂O₃, and V₂O₅ [3, 12-23]. In this context, this mini review presents a summary of recent developments in vanadium oxide based supercapacitor along with future developments, prospects, and challenges.

2. Electrochemical properties of vanadium dioxide:

Vanadium dioxide (VO₂) is known to be stabilized in different polymorphs, including VO₂(A), VO₂(B), VO₂(C), VO₂(D), among others. [24]. Among the VO₂ polymorphs, VO₂(B) attracted much attention for its well known MIT at a technologically important temperature of 340K, which is very close to room temperature [25]. VO₂(B) crystallizes in rutile tetragonal (R; space group *P4₂/mnm*) and monoclinic (M1; space group *P2₁/c*) structure above and below the transition temperature, respectively [26,27]. In the high-temperature R phase, V atoms are equally spaced, forming linear chains along the *c_R* axis with each V atom surrounded by an oxygen octahedron [28]. The lattice parameters are *c_R* = 2.85 Å, and *a_R* = *b_R* = 4.55 Å. Whereas in the low-temperature monoclinic phase the volume of the unit cell becomes double than that of R phase with lattice parameters *a_{M1}* = 5.70 Å, *b_{M1}* = 4.55 Å, *c_{M1}* = 5.38 Å, and *β_{M1}* = 123° [29]. The approximate crystallographic relationship between M1 and R phase is *a_{M1}* ↔ 2*c_R*, *b_{M1}* ↔ *a_R*, and *c_{M1}* ↔ *b_R* - *c_R* [30]. In the M1 phase, there are significant differences in the arrangement of V along *c_R* axis. The V atoms form pair, and the pairs tilt along the *c_R* axis making the surrounding octahedron deformed. Besides M1, two more metastable phases of monoclinic M2 having space group *C2/m* and triclinic T (alternatively monoclinic M3) with space group *C₁* are also reported in the process of the phase transition from M1 to R [31].

There are several reports on the supercapacitive performance of VO₂(B) in the M1 phase. However, its low rate capability and cycling instability become the obstacles to serve as a

commercial supercapacitor. The modification in structure designing has been adopted to overcome the barrier. Zhang *et al.* [32] prepared a template-free 3D hollow spherical cages (shown in figures 1a-b) by hydrothermal method, which showed a specific capacitance of $1175 \text{ mF} \cdot \text{cm}^{-2}$ ($336 \text{ F} \cdot \text{g}^{-1}$) with enhanced stability, and 68% of the capacitance was retained after 10000 cycles. However, 2D nanosheet of VO_2 is reported to be a more eligible candidate for electrochemical performance than that of 3D counterpart because of large specific surface area shortening the diffusion path of ion and enhance the redox reaction. Ndiaye *et al.* [33] obtained specific capacitance of $663 \text{ F} \cdot \text{g}^{-1}$ at the scan rate of $5 \text{ mV} \cdot \text{s}^{-1}$ and excellent cycling stability after 5000 cycles at the current density of $10 \text{ A} \cdot \text{g}^{-1}$ for VO_2 nanosheets. The 2D nanosheets (figures 1c-d), while assembled with the structure of carbonized iron-polyaniline (C-FP), exhibited a specific capacity of $47 \text{ mAh} \cdot \text{g}^{-1}$ at a current density of $1 \text{ A} \cdot \text{g}^{-1}$ [34]. In 2D nanosheets, a large specific surface area diminishes the path length of the ion diffusion enabling the execution of the redox reaction effectively. Rakhi *et al.* [35] reported a specific capacitance of $\sim 405 \text{ F} \cdot \text{g}^{-1}$ at the current density of $1 \text{ A} \cdot \text{g}^{-1}$ of VO_2 nanosheets in an organic gel electrolyte (1 M LiClO_4 in propylene carbonate) with nearly 82% capacitance retention.

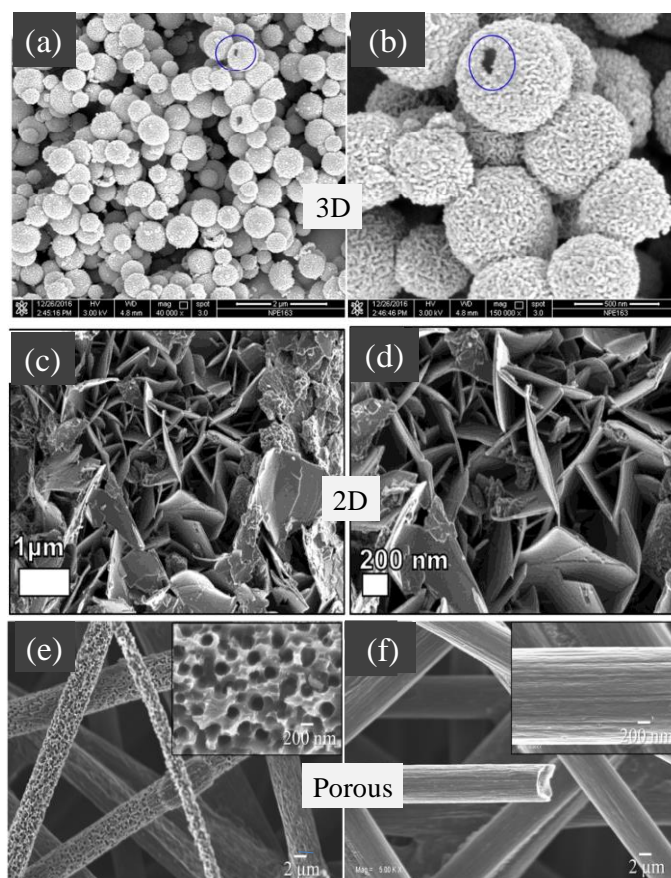


Figure 1. Scanning electron micrograph of (a-b) VO₂ 3D hollow spherical cages and its higher magnification image; marked circles shows broken area [Reprinted with permission from Ref. 33, Copyright 2018 @ Royal Society of Chemistry] (c-d) 2D VO₂ nanosheets and its zoomed image [Reprinted with permission of authors from Ref. 34, Copyright 2019 @ American Institute of Physics], (e) VO₂ nanoporous structure grown on carbon paper, (f) bare C fiber [Reprinted with permission of authors from Ref. 37, Copyright 2019 @ Nature Publishing Group].

The thin layer of 1D VO₂ nanorods on indium tin oxide - coated glass substrates are also reported [36] to produce a specific capacitance of $\sim 486 \text{ mF} \cdot \text{cm}^{-2}$ at the scan rate of $10 \text{ mV} \cdot \text{s}^{-1}$. Nie *et al.* [19] reported VO₂@Polyaniline coaxial nanobelts exhibiting a higher specific capacitance of $246 \text{ F} \cdot \text{g}^{-1}$ at $0.5 \text{ A} \cdot \text{g}^{-1}$ than that of VO₂ nanobelts ($160.9 \text{ F} \cdot \text{g}^{-1}$). The specific capacitance was almost constant at around $118 \text{ mF} \cdot \text{cm}^{-2}$ after 5000 cycles at the scan rate of $100 \text{ mV} \cdot \text{s}^{-1}$. VO₂ nanoporous structures on carbon fiber in the M1 phase (figures 1e-f) exhibit a specific capacitance of 20.7

$\text{mF}\cdot\text{cm}^{-2}$ at the current density of $0.3\text{ mA}\cdot\text{cm}^{-2}$ [37]. It also demonstrates capacitance retention of 93.7% and coulombic efficiency of 98.2% for 5000 charge-discharge cycles. However, the similar nanoporous structures in M2 and T phases of VO_2 show poor specific capacitance (figure 2a) as well as cyclic stability (figure 2b) because of mixed valency [37].

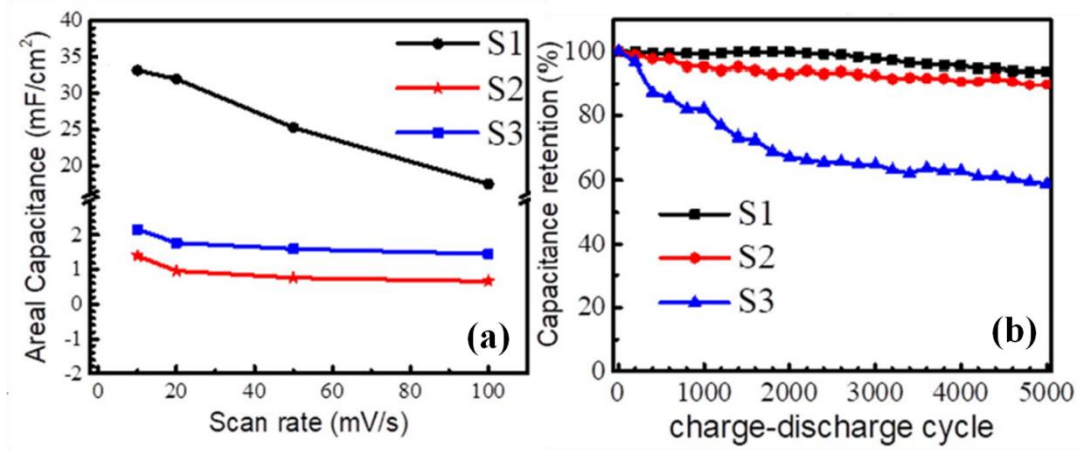


Figure 2. (a) Areal capacitance versus scan rate and (b) capacitance retention with charge-discharge cycle of pure M1 (S1), and mixed phases of VO_2 (S2 and S3) [Reprinted with permission of authors from Ref. 37, Copyright 2019 @ Nature Publishing Group].

Another way to enhance the electrochemical performance of VO_2 is by combining with carbon materials, which improve the electrical conductivity. VO_2 nanoflowers on 3D graphene networks were reported to exhibit a large specific capacitance of $466\text{ mF}\cdot\text{cm}^{-2}$, capacitance retention of 63.5% after 3000 cycles by Wang *et al.* [38]. Ren *et al.* [39] synthesized VO_2 nanoparticles on edge-oriented graphene foam (EOGF) which exhibit a capacitance of $119\text{ mF}\cdot\text{cm}^{-2}$ at the scan rate of $2\text{ mV}\cdot\text{s}^{-1}$. The $\text{VO}_2(\text{B})$ /carbon core-shell composites prepared by Zhang *et al.* [40] exhibited a specific capacitance of $203\text{ F}\cdot\text{g}^{-1}$ at the current density of $0.2\text{ A}\cdot\text{g}^{-1}$. Lv *et al.* [41] prepared $\text{VO}_2(\text{B})$ nanobelts/rGO composites with a porous framework, which showed an excellent power density of $7152\text{ W}\cdot\text{kg}^{-1}$ at the energy density of $3.13\text{ Wh}\cdot\text{kg}^{-1}$. Shao *et al.* [20] reported VO_2 demonstrating superior properties as supercapacitor compared to that for the V_2O_5 , which was well known for its

SC performance. It is due to higher electronic conductivity in VO_2 , as compared to V_2O_5 , originating from a mixed-valence and structural stability because of the increased edge sharing and the consequent resistance to lattice shearing during cycling [42]. The comparison of various VO_2 based supercapacitors and their synthesis procedures are shown in table 1.

3. Electrochemical properties of vanadium trioxide:

Vanadium trioxide (V_2O_3) reveals a rhombohedral corundum structure at room temperature, (space group $R\bar{3}c$) [43], where the V atoms pair along the crystal c -axis and form honeycomb lattices in the ab -plane. Whereas, below the temperature ~ 150 K, a paramagnetic metallic to an antiferromagnetic insulating transition happens along with the structural transition to the monoclinic phase (space group I_2/a) [44].

There are very few reports on the electrochemical studies on V_2O_3 , mostly because of the poor stability of this material. A binder-free electrode of V_2O_3 nanoflakes on N-doped rGO (figure 3a) was reported to have an areal capacitance of $216 \text{ mF}\cdot\text{cm}^{-2}$ at a current density of $1 \text{ mA}\cdot\text{cm}^{-2}$ (figure 3b). It also exhibits cycling stability with retention of $\sim 81\%$ of the initial capacitance value after 10000 cycles (figure 3c) [45].

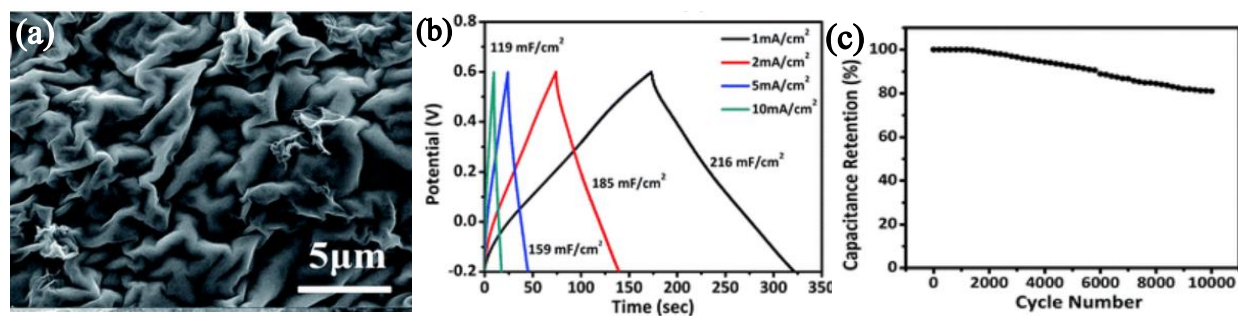


Figure 3. (a) Scanning electron micrograph of the $\text{V}_2\text{O}_3/\text{N-rGO}$ samples, (b) The galvanostatic charge-discharge (GCD) curves obtained for the self-supported $\text{V}_2\text{O}_3/\text{N-rGO}$ film electrodes at different current densities. (c) Cycling stability for 10000 cycles [Reprinted with permission from Ref. 45, Copyright 2017 @ Royal Society of Chemistry].

Table1: Comparison of various VO₂ based supercapacitors

Nanostructures (Growth Technique)	Electrolyte	Specific Capacitance	Current density	Cycling stability (%)	Ref.
VO ₂ (B) hollow spheres (Solvothermal)	1 M Na ₂ SO ₄ / critical micelle concentration	336 F·g ⁻¹	2 mA·cm ⁻²	68% (10000 cycles)	33
VO ₂ nanosheets (Solvothermal)	6 M KOH	663 F·g ⁻¹	10 A·g ⁻¹	99.4% (9000 cycles)	34
VO ₂ nanosheets (Solvothermal)	6 M KOH	47 mAh·g ⁻¹	1 A·g ⁻¹	89% (10 000 cycles)	34
VO ₂ nanosheet (Solution Reduction of hydrothermally exfoliated bulk V ₂ O ₅)	1 M LiClO ₄ /PPC	405 F·g ⁻¹	1 A·g ⁻¹	82% (6000 cycles)	35
VO ₂ nanorod thin films (RF magnetron sputtering)	0.1 M NaOH	486 mF·cm ⁻²	10 mV·s ⁻¹	100% (5000 cycles)	36
VO ₂ @Polyaniline coaxial nanobelts (Reactive templated organic layer on solvothermally grown VO ₂ nanobelt)	0.5 M Na ₂ SO ₄	246 F g ⁻¹ .	0.5 A g ⁻¹	(28.6%) (1000 cycles)	19
Nanoporous VO ₂ (Vapour transport of bulk V ₂ O ₅ on C-paper)	Na ₂ SO ₄	20.7 mF·cm ⁻²	0.3 mA·cm ⁻²	93.7% (5000 cycles)	37
VO ₂ NFs@3DG (Hydrothermally grown VO ₂ on 3DG)	0.5 M K ₂ SO ₄	507 F·g ⁻¹	3 mA·cm ⁻²	63.5% (3000 cycles)	38
VO ₂ nanoparticle/EOGF (Hydrothermally grown VO ₂ on EOGF)	5 M LiCl	119 mF·cm ⁻²	2 mV·s ⁻¹	70% (1500 cycles)	39
VO ₂ (B)/C core-shell (Single pot hydrothermal)	1 M Na ₂ SO ₄	203 F·g ⁻¹	0.2 A·g ⁻¹	10.4% (100 cycles)	40
VO ₂ (B) nanobelts/rGO (Hydrothermally grown VO ₂ on rGO)	0.5 M K ₂ SO ₄	353 F·g ⁻¹	1 A·g ⁻¹	78% (10 000 cycles)	41

However, V₂O₃ combined with carbon composites are reported to serve as superior electrode material. Zheng *et al.* reported V₂O₃/C composites exhibiting high pseudocapacitance of 458.6

$\text{F} \cdot \text{g}^{-1}$ at $0.5 \text{ A} \cdot \text{g}^{-1}$. The composite also shows a retention rate of 86% after 1000 cycles in aqueous electrolyte [46]. Hu *et al.* [47] synthesized $\text{V}_2\text{O}_3/\text{C}$ core-shell nanorods with porous structures which exhibited 228, 221, 207, 158, and $127 \text{ F} \cdot \text{g}^{-1}$ specific capacitances at current densities of 0.5, 1, 2, 5, and $10 \text{ A} \cdot \text{g}^{-1}$, respectively. Zhang *et al.* [48] reported a V_2O_3 nanofoam@activated carbon composite, which showed a specific capacitance of $185 \text{ F} \cdot \text{g}^{-1}$ at $0.05 \text{ A} \cdot \text{g}^{-1}$. The comparison of various V_2O_3 based supercapacitors, fabricated following different process steps, are shown in table 2.

Table 2: Comparison of various V_2O_3 based supercapacitors

Nanostructures (Growth Technique)	Electrolyte	Specific Capacitance	Current density	Cycling stability (%)	Ref.
$\text{V}_2\text{O}_3/\text{N-rGO}$ nanoflakes (500°C NH_3 reduction of V_2O_5 gel/GO films)	1 M Na_2SO_4	216 $\text{mF} \cdot \text{cm}^{-2}$	$1 \text{ mA} \cdot \text{cm}^{-2}$	81% (10000 cycles)	45
$\text{V}_2\text{O}_3/\text{C}$ nanocomposites (Calcination of hydrothermally grown $(\text{NH}_4)_2\text{V}_3\text{O}_8$)	5 M LiCl	$458.6 \text{ F} \cdot \text{g}^{-1}$	$0.5 \text{ A} \cdot \text{g}^{-1}$	86% (1000 cycles)	46
$\text{V}_2\text{O}_3/\text{C}$ core-shell nanorods (Single pot hydrothermal process using V_2O_5 nanorod)	5 M LiCl	$228 \text{ F} \cdot \text{g}^{-1}$	$0.5 \text{ A} \cdot \text{g}^{-1}$	86% (1000 cycles)	47
V_2O_3 nanofoam@activated carbon (Calcination of NH_4VO_3 solution and activated C)	1 M NaNO_3	$185 \text{ F} \cdot \text{g}^{-1}$	$0.05 \text{ A} \cdot \text{g}^{-1}$	49% (100 cycles)	48

4. Electrochemical properties of vanadium pentoxide:

Vanadium pentoxide (V_2O_5) stabilizes in various phases including $\alpha\text{-V}_2\text{O}_5$, $\beta\text{-V}_2\text{O}_5$, $\delta\text{-V}_2\text{O}_5$, $\gamma'\text{-V}_2\text{O}_5$, $\zeta\text{-V}_2\text{O}_5$, and $\varepsilon'\text{-V}_2\text{O}_5$ [49]. The most well-known phase is $\alpha\text{-V}_2\text{O}_5$, which crystallizes into an orthorhombic structure composed of weakly Van der Waals bonded layers of VO_5 pyramids sharing their vertices and corners [50,51]. The unit-cell parameters are $a = 11.51 \text{ \AA}$, $b = 3.56 \text{ \AA}$,

and $c = 4.37 \text{ \AA}$ [50]. It has space group $Pmmn$, (D_{2h}^{13}) with distorted square-pyramidal coordination symmetry around each V atom. There are three non-equivalent oxygen atoms in each unit cell (denoted as O_I , O_{II} , and O_{III}). O_I is the terminal (vanadyl) oxygen with two different bond lengths. One of them is a strong and short V- O_I bond with a length of 1.577 \AA (d_1). Another one is large and weak Van der Waals type connecting two adjacent layers in the V_2O_5 structure, with a bond length of 2.793 \AA . Both of these O_I atoms orient almost along the c -axis. The two-fold coordinated bridging oxygen (O_{II}) connects two adjacent V atoms with V- O_{II} bond length of 1.78 \AA (d_2). The ladder-shaped O_{III} atoms are the three-fold coordinated oxygen with three different V- O_{III} bond lengths of 1.88 \AA (d_3), 1.88 \AA (d_3), and 2.02 \AA (d_4) [50].

The SC properties in V_2O_5 is reported to be superior to other vanadium oxides because of its stability and layered structure [16,18,19,20]. Yang *et al.* [52] prepared hollow V_2O_5 spheres which showed an excellent capacitance of $479 \text{ F}\cdot\text{g}^{-1}$ at $5 \text{ mV}\cdot\text{s}^{-1}$. V_2O_5 nanofibers showed specific capacitance of $190 \text{ F}\cdot\text{g}^{-1}$ in aqueous electrolyte (KCl) and $250 \text{ F}\cdot\text{g}^{-1}$ in the organic electrolyte (LiClO_4 in PPC) as reported by Wee *et al.* [53]. Apart from supercapacitor performance, the change in electrolytes in case of V_2O_5 also controls its mechanical stability and chemical dissolution. Pandit *et al.* [54] synthesized V_2O_5 thin film on a pliable stainless steel substrate which is reported to exhibit a high specific capacitance of $735 \text{ F}\cdot\text{g}^{-1}$ at $1 \text{ mV}\cdot\text{s}^{-1}$ with capacitors retention of 71% after 1000 cycles.

The rGO/ V_2O_5 composites showed specific capacitance of 386, 338, 294, 241, and 197 $\text{F}\cdot\text{g}^{-1}$ at current density of 0.1, 0.2, 0.5, 1, and 2 $\text{A}\cdot\text{g}^{-1}$, respectively, as reported by Liu *et al.* [55]. However, 2D heterostructures of V_2O_5 nanosheets growing on rGO flakes showed relatively high specific capacitance of $653 \text{ F}\cdot\text{g}^{-1}$ at $1 \text{ A}\cdot\text{g}^{-1}$ and cyclic stability of 94% after 3000 cycles [56]. Choudhury *et al.* [57] prepared V_2O_5 nanofiber (VNF)/exfoliated graphene nanohybrid with the

mass ratio of 1:0.25 and 1:0.5 with a superior capacitance value of $218 \text{ F} \cdot \text{g}^{-1}$ at $1 \text{ A} \cdot \text{g}^{-1}$ for 1:0.5 mass ratio. Balasubramanian *et al.* [58] reported flowery V_2O_5 structures coated with carbon showing specific capacitance of $417 \text{ F} \cdot \text{g}^{-1}$ at a current density of $0.5 \text{ A} \cdot \text{g}^{-1}$. Chen *et al.* [59] synthesized V_2O_5 nanocomposites with carbon nanotubes (CNT) which provided a capacity of $228 \text{ C} \cdot \text{g}^{-1}$ between 1.8 and 4.0 V. Wu *et al.* [60] reported V_2O_5 /multi-walled CNT core/shell hybrid aerogel (figure 4a), which demonstrated the maximum specific capacitance of $625 \text{ F} \cdot \text{g}^{-1}$ with outstanding cycle performance (>20000 cycles). The hybrid aerogel showed better performance than that of raw V_2O_5 powder, MWCNTs, and V_2O_5 aerogel (figure 4b).

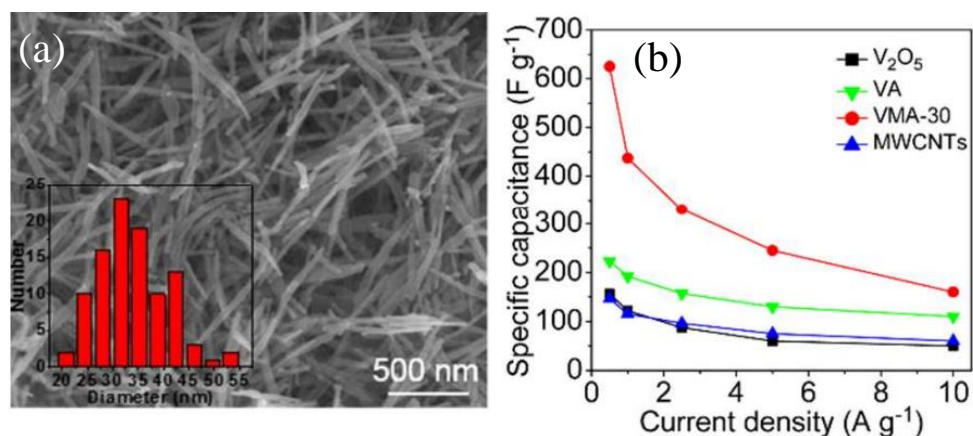


Figure 4. (a) Scanning electron micrograph of V_2O_5 aerogel and diameter distribution of V_2O_5 nanofibers (inset) (b) Specific capacitance as a function of current density for raw V_2O_5 powder, MWCNTs, V_2O_5 aerogel and hybrid aerogel of $\text{V}_2\text{O}_5/\text{C}$ nanocomposites (VMA-30) [Reprinted with permission from Ref. 60, Copyright 2015 @ Royal Society of Chemistry].

However, the insertion of nitrogen atoms into the carbon network enhances the electrochemical performance by restraining the hydrophobicity. Sun *et al.* [61] reported self-assembled 3D N-carbon nanofibers (CNFs)/ V_2O_5 aerogels showing the specific capacitance of $575.6 \text{ F} \cdot \text{g}^{-1}$ even after 12000 cycles (97% of the initial value). V_2O_5 also have been combined with conducting polymers *e.g.*, polypyrrole (PPy), poly (3, 4-ethylenedioxythiophene) (PEDOT), and

polyaniline (PANI), to enhance the electrical conductivity and prevent the V from dissolving. Qian *et al.* [62] reported 3D V_2O_5 /PPy nanostructures, which exhibited a high specific capacitance of $448 \text{ F}\cdot\text{g}^{-1}$. However, Bi *et al.* [63] showed a comparative study with oxygen vacancy (\ddot{O}) resulting with the specific capacitance of $614 \text{ F}\cdot\text{g}^{-1}$ for $V\ddot{O}$ - V_2O_5 /PEDOT higher than that of $523 \text{ F}\cdot\text{g}^{-1}$ for $V\ddot{O}$ - V_2O_5 /PANI and $437 \text{ F}\cdot\text{g}^{-1}$ for $V\ddot{O}$ - V_2O_5 /PPy (figures 5a-b).

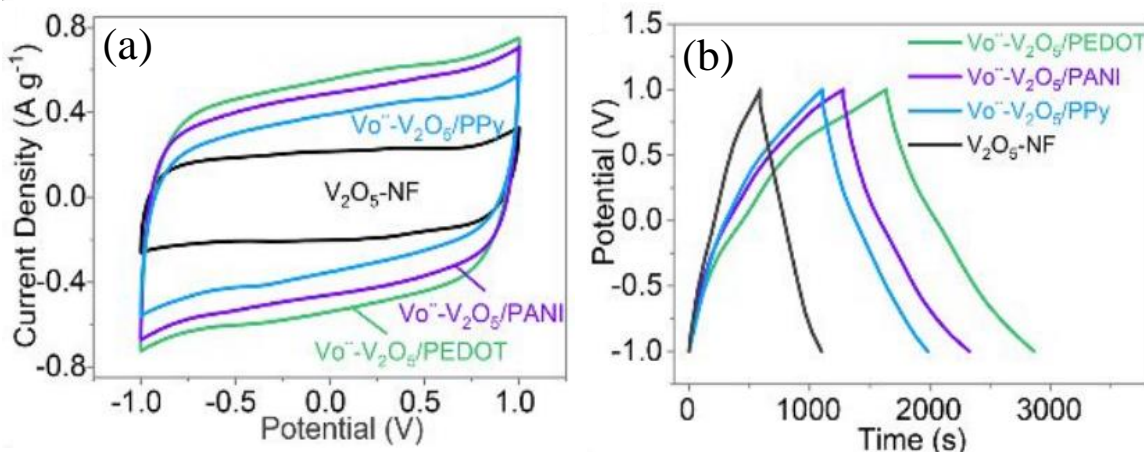


Figure 5. (a) CV curves of $V\ddot{O}$ - V_2O_5 /Conducting polymers and V_2O_5 -NF at a scan rate of 5 mV s^{-1} . (b) galvanostatic charge-discharge curves of $V\ddot{O}$ - V_2O_5 /Conducting polymers and V_2O_5 -NF at a current density of $0.5 \text{ A}\cdot\text{g}^{-1}$ [Reprinted with permission from Ref. 63, Copyright 2019 @ Royal Society of Chemistry].

The association of V_2O_5 with other metal oxides is also reported to enhance the electrochemical properties. Xu *et al.* prepared V_2O_5 nanobelts/ TiO_2 nanoflakes composites [64], which exhibited high specific capacitance of $587 \text{ F}\cdot\text{g}^{-1}$ at $0.5 \text{ A}\cdot\text{g}^{-1}$ with good cyclic stability of 97% after 5000 cycles. The V_2O_5 -doped $\alpha\text{-Fe}_2O_3$ composites by Nie *et al.* [65] showed a capacitance value of $150 \text{ F}\cdot\text{g}^{-1}$ over 200 cycles at $6 \text{ A}\cdot\text{g}^{-1}$. CNT- SnO_2 - V_2O_5 composites exhibited higher specific capacitance compared to CNT, V_2O_5 , and CNT- V_2O_5 [66]. V_2O_5 shows higher performance combined with carbon and other metal oxides than that of the other two phases of vanadium oxides discussed before. The comparison of various V_2O_5 based supercapacitors with involved synthesis techniques are shown in table 3.

Table 3: Comparison of various V₂O₅ based supercapacitors

Nanostructures (Growth Technique)	Electrolyte	Specific Capacitance	Current density	Cycling stability (%)	Ref.
Hollow spherical V ₂ O ₅ (Solvothermal)	5 M LiNO ₃	479 F·g ⁻¹	5 mV·s ⁻¹	43% (100 cycles)	52
V ₂ O ₅ nanofibers (Electrospinning)	(i) 2 M KCl (ii) 1 M LiClO ₄ /PPC	190 F·g ⁻¹ 250 F·g ⁻¹	0.1 A·g ⁻¹		53
V ₂ O ₅ complex (Chemical bath deposition)	2 M LiClO ₄	735 F·g ⁻¹	1 mV·s ⁻¹	71% (1000 cycles)	54
rGO/V ₂ O ₅ hybrid aerogel (One-pot Hydrothermally grown)	1 M LiClO ₄ /PPC	384 F·g ⁻¹	0.1 A·g ⁻¹	82.2% (10 000 cycles)	55
rGO/V ₂ O ₅ nanosheet (Mixing rGO with hydrothermally grown V ₂ O ₅)	1 M KCl	653 F·g ⁻¹	1 A·g ⁻¹	94% (3000 cycles)	56
VNF/graphene nanohybrid (Hydrothermally grown VNF mixed with exfoliated graphene)	1 M LiTFSI in acetonitrile	218 F·g ⁻¹	1 A·g ⁻¹	87% (700 cycles)	57
Carbon coated flower V ₂ O ₅ (Co-precipitation method followed by annealing at 400 °C)	1 M K ₂ SO ₄	417 F·g ⁻¹	0.5 A·g ⁻¹	100% (2000 cycles)	58
CNT/V ₂ O ₅ nanocomposite (One-pot hydrothermal process of V ₂ O ₅ and hydrophilic CNTs)	1 M LiClO ₄ /PPC	228 C·g ⁻¹	20 mV·s ⁻¹	80% (10000 cycles)	59
V ₂ O ₅ /MWCNT core/shell hybrid aerogels (One-step sol-gel process)	1 M Na ₂ SO ₄	625 F·g ⁻¹	0.5 A·g ⁻¹	120% (20 000 cycles)	60
3D N-CNFs/V ₂ O ₅ aerogels (Self-assembly of nanostructured V ₂ O ₅ onto CNF aerogels with N)	1 M Na ₂ SO ₄	595.1 F·g ⁻¹	0.5 A·g ⁻¹	97% (12000 cycles)	61
3D V ₂ O ₅ /PPy core/shell nanostructures (V ₂ O ₅ by ion exchange attached with PPy)	5 M LiNO ₃	448 F·g ⁻¹	0.5 A·g ⁻¹	81% (1000 cycles)	62
V ₂ O ₅ -Conductive polymer nanocables (V ₂ O ₅ sol attached to functionalized polymers)	1 M Na ₂ SO ₄	614 F·g ⁻¹	0.5 A·g ⁻¹	111% (15 000 cycles)	63
V ₂ O ₅ /TiO ₂ composites (Two-step hydrothermal process using Ni foam)	1 M LiNO ₃	587 F·g ⁻¹	0.5 A·g ⁻¹	92% (1000 cycles)	64
V ₂ O ₅ -α-Fe ₂ O ₃ composite nanotubes (One-step electrospinning)	3 M KOH	183 F·g ⁻¹	1 A·g ⁻¹	81.5% (200 cycles)	65
SnO ₂ -V ₂ O ₅ -CNT (One-pot hydrothermal)	0.1 M KCl	121.39 F·g ⁻¹	100 mV·s ⁻¹	85.8% (100 cycles)	66

Large scale production, however, can perhaps be considered for the most stable phase of V_2O_5 with its optimum performance as a supercapacitor. Thus, looking into the economic prospect, materials involving sol-gel route synthesis [60, 63, 67] and electrospinning [53] may be adopted for the growth of various V_2O_5 .

5. Electrochemical properties of VO_x :

Other than the stoichiometric oxides of V, there are also reports of electrochemical applications of multi-valent vanadium oxides (VO_x). The V-O phase diagram comprises mixed-valence oxides comprehending two oxidation states, namely, V_3O_7 , V_6O_{13} , V_8O_{15} , V_7O_{13} , V_6O_{11} , among others [68]. It permits conversion between oxides of different stoichiometry. Huang *et al.* [69] reported a high areal capacitance of $1.31 \text{ F}\cdot\text{cm}^{-2}$ from VO_x functionalized by a carbon nanowire array. V_3O_7 was reported to get converted to V_6O_{13} at the lowest potential of -0.6 V and V_2O_5 at the highest potential of 0.2 V. Zhao *et al.* [70] prepared NC-coated nest-like V_3O_7 which showed the specific capacity of $660.63 \text{ F}\cdot\text{g}^{-1}$ at $0.5 \text{ A}\cdot\text{g}^{-1}$ (figure 6a), a significantly higher than that of V_3O_7 ($362.63 \text{ F}\cdot\text{g}^{-1}$). NC- V_3O_7 exhibited 80.47% of the initial capacitance at $10 \text{ A}\cdot\text{g}^{-1}$ after 4000 cycles, which is 23.16% higher than that of V_3O_7 (figure 6b).

V_6O_{13} has stimulated extensive attention owing to its high specific capacitance and decent cycle ability for Li batteries. However, there are very few reports on its SC performance. V_6O_{13} is known as a mixed-valence oxide as it exists between the V^{4+} and V^{5+} oxidation states with 2:1 ratio [71], which increases the electronic conductivity of the material. Zhai *et al.* [72] reported V_6O_{13} as well as sulfur-doped, oxygen-deficient V_6O_{13-x} as an anode electrode.

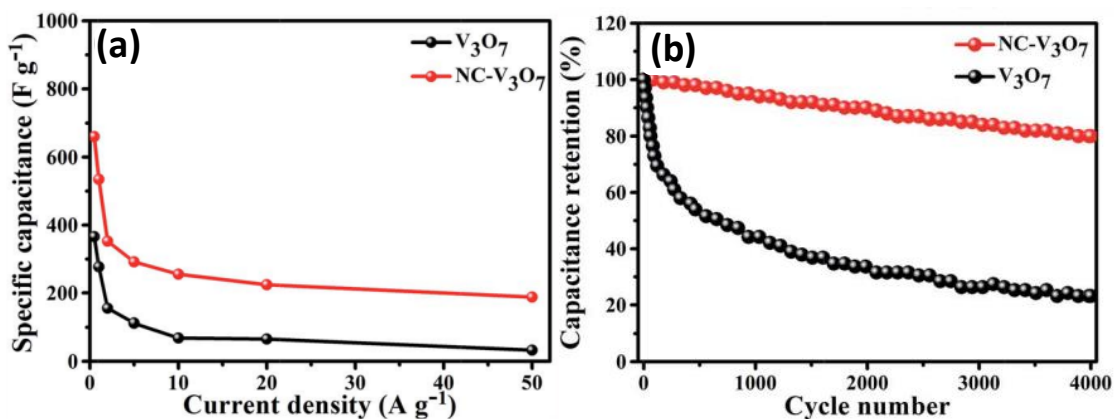


Figure 6. (a) Specific capacitance of V₃O₇ and NC-V₃O₇ as a function of current density and (b) cycling performance of V₃O₇ and NC-V₃O₇ at a current density of 10 A g⁻¹ [Reprinted with permission from Ref. 69, Copyright 2019 @ Royal Society of Chemistry].

V₆O_{13-x} provides a capacitance of 1353 F·g⁻¹ at a current density of 1.9 A·g⁻¹ and outstanding capacitance retention of 92.3% after 10000 cycles. Pang *et al.* [73] reported the high electrochemical performance of 3D microflower structure of V₄O₉ supercapacitors (~392 F·g⁻¹).

6. Conclusion and outlook:

This brief review deals with the electrochemical performances of vanadium oxides and its composites as supercapacitors. Vanadium oxides have attracted tremendous attention in electrochemistry due to their multi-valency, low cost and abundant sources on earth. However, poor electrical conductivity, structural instability, poor specific capacitance and low energy density limit their practical applications. The scientific community is working towards removing the obstacles by morphology engineering (increase the specific surface area), doping with a heteroatom (reduce hydrophobicity and structural stability), combined with carbon-based materials and/or conducting polymers (increasing conductivity) and so on. The structure designing

increases the specific surface area and offer more active sites which intern increases the contact between the material and electrolyte, generates more redox reactions, and enhances the electrochemical performance of the materials. It has been observed from the previous studies that nanostructures with porosity are the best choice for increasing supercapacitive performance. On the other hand, combining with composites increases the specific capacity, cyclic stability, and finally energy and power density. Comments are also made for the commercial viability in terms of large area synthesis of a stable phase of vanadium oxide with optimized supercapacitance properties. Finding a proper composite material for a specific vanadium oxide is still a challenge for future development. Finally, as vanadium oxides are prone to change the oxidization state, in-situ characterization techniques are likely to be carried out during the electrochemical processes. Most of the vanadium oxides also undergo electrical, magnetic, and/or structural transition with minimal change in the electric field, temperature, or pressure. Therefore, to understand the change in phases and its role in the electrochemical process, advanced in-situ characterization techniques should be incorporated.

References:

1. Inagaki M, Konno H, Tanaike O. Carbon materials for electrochemical capacitors. *J. Power Sources* 2010;195:7880-7903.
2. Lokhande C, Dubal D, Joo O.-S. Metal oxide thin film based supercapacitors. *Curr. Appl. Phys.* 2011;11:255-270.
3. Shown I, Ganguly A, Chen LC, Chen KH. Conducting polymer-based flexible supercapacitor. *Energy Science & Engineering* 2015;3:2-26.

4. Zhao T, Ji X, Bi P, Jin W, Xiong C, Dang A, Li H, Li T, Shang S, Zhou Z. In situ synthesis of interlinked three-dimensional graphene foam/polyaniline nanorods supercapacitor. *Electrochim. Acta* 2017;230:342-349.
5. Zhou Z, Zhang Q, Sun J, He B, Guo J, Li Q, Li C, Xie L, Yao Y. Metal-organic framework derived spindle-like carbon incorporated α -Fe₂O₃ grown on carbon nanotube fiber as anodes for high-performance wearable asymmetric supercapacitors. *ACS Nano* 2018;12:9333-9341.
6. Zhang Q, Xu W, Sun J, Pan Z, Zhao J, Wang X, Zhang J, Man P, Guo J, Zhou Z, He B, Zhang Z, Li Q, Zhang Y, Xu L, Yao, Y. Constructing ultrahigh-capacity zinc–nickel–cobalt oxide@Ni(OH)₂ core-shell nanowire arrays for high-performance coaxial fiber-shaped asymmetric supercapacitors. *Nano lett.* 2017;17:7552-7560.
7. Zhang Q, Sun J, Pan Z, Zhang J, Zhao J, Wang X, Zhang C, Yao Y, Lu W, Li Q, Zhang, Y, Zhang, Z. Stretchable fiber-shaped asymmetric supercapacitors with ultrahigh energy density. *Nano Energy* 2017;39:219-228.
8. Yan Y, Li B, Guo W, Pang H, Xue H. Vanadium based materials as electrode materials for high performance supercapacitors. *J. Power Sources* 2016;329:148-169.
9. Man P, Zhang Q, Sun J, Guo J, Wang X, Zhou Z, He B, Li Q, Xie L, Zhao J, Li C, Li Q, Yao, Y. Hierarchically structured VO₂@PPy core-shell nanowire arrays grown on carbon nanotube fibers as advanced cathodes for high-performance wearable asymmetric supercapacitors. *Carbon* 2018;139:21-28.
10. Zhang Q, Wang X, Pan Z, Sun J, Zhao J, Zhang J, Zhang C, Tang L, Luo J, Song B, Zhang Z, Lu W, Li Q, Zhang Y, Yao Y. Wrapping aligned carbon nanotube composite sheets around vanadium nitride nanowire arrays for asymmetric coaxial fiber-shaped supercapacitors with ultrahigh energy density. *Nano lett.* 2017;17:2719-2726.

11. Haber J. Fifty years of my romance with vanadium oxide catalysts. *Catal. Today* 2009;142:100-113.
12. Ma, XJ, Zhang WB, Kong LB, Luo YC. Kang, L. VO₂: From negative electrode material to symmetric electrochemical capacitor. *RSC Adv.* 2015;5:97239-97247.
13. Hu C, Xu H, Liu X, Zou F, Qie L, Huang Y. Hu, X. VO₂/TiO₂ nanosponges as binder-free electrodes for high-performance supercapacitors. *Sci. Rep.* 2015;5:16012.
14. Lee M, Wee BH, Hong JD. High performance flexible supercapacitor electrodes composed of ultralarge graphene sheets and vanadium dioxide. *Adv. Energy Mater.* 2015;5:1401890.
15. Senthilkumar ST, Selvan RK, Ponpandian N, Meloc JS, Leed, YS. Improved performance of electric double layer capacitor using redox additive (VO²⁺/VO₂⁺) aqueous electrolyte. *J. Mater. Chem. A* 2013;1:7913-7919.
16. Huang G, Li C, Sun X, Bai J. Fabrication of vanadium oxide, with different valences of vanadium, -embedded carbon fibers and their electrochemical performance for supercapacitor. *New J. Chem.* 2017;41:8977-8984.
17. Tang K, Li Y, Li Y, Cao H, Zhang Z, Zhang Y, Yang, J. Self-reduced VO/VO_x/carbon nanofiber composite as binder-free electrode for supercapacitors. *Electrochim. Acta* 2016;209:709-718.
18. Wang J, Zhang X, Zhang Y, Abas A, Zhao X, Yang Z, Su Q, Lan W, Xie, E. Lightweight, interconnected VO₂ nanoflowers hydrothermally grown on 3D graphene networks for wide-voltage-window supercapacitors. *RSC Adv.* 2017;7:35558-35564.
19. Nie G, Lu X, Zhu Y, Chi M, Gao M, Chen S, Wang, C. Reactive template synthesis of inorganic/organic VO₂@Polyaniline coaxial nanobelts for high-performance supercapacitors. *ChemElectroChem* 2017;4:1095-1100.

20. Shao J, Li X, Qu Q, Zheng, H. One-step hydrothermal synthesis of hexangular starfruit-like vanadium oxide for high power aqueous supercapacitors. *J. Power Sources* 2012;219:253-257.
21. Hu L, Yu L, Zhao C, Long X, Chen, W. Synthesis and characterization of VO₂/mesoporous carbon composites for hybrid capacitors. *J. Wuhan Univ. Technol.-Mat. Sci. Edit.* 2010;25:574-578.
22. Li M, Sun G, Yin P, Ruan C, Ai K. Controlling the formation of rodlike V₂O₅ nanocrystals on reduced graphene oxide for high-performance supercapacitors. *ACS Appl. Mater. Interfaces* 2013;5:11462-11470.
23. Zhu J, Cao L, Wu Y, Gong Y, Liu Z, Hoster HE, Zhang Y, Zhang S, Yang S, Yan Q, Ajayan PM, Vajtai R. Building 3D structures of vanadium pentoxide nanosheets and application as electrodes in supercapacitors. *Nano Lett.* 2013;13:5408-5413.
24. Srivastava A, Rotella H, Saha S, Pal B, Kalon G, Mathew S, Motapothula M, Dykas M, Yang P, Okunishi E, Sarma DD, Venkatesan T. Selective growth of single phase VO₂ (A, B, and M) polymorph. *Thin Films. APL Mater.* 2015;3:026101.
25. Morin FJ. Oxides which show a metal-to-insulator transition at the Neel temperature. *Phys. Rev. Lett.* 1959;3:34.
26. Haverkort MW, Hu Z, Tanaka A, Reichelt W, Streltsov SV, Korotin MA, Anisimov VI, Hsieh, HH, Lin HJ, Chen CT, Khomskii DI, Tjeng LH. Orbital-assisted metal-insulator transition in VO₂. *Phys. Rev. Lett.* 2005;95:196404.
27. Kim, HT, Lee YW, Kim BJ, Chae BG, Yun SJ, Kang KY, Han K, Yee KJ, Lim YS. Monoclinic and correlated metal phase in VO₂ as evidence of the Mott transition: Coherent phonon analysis. *Phys. Rev. Lett.* 2006;97:266401.

28. Zylbersztein A, Mott NF. Metal-insulator transition in vanadium dioxide. *Phys. Rev. B*, 1975;11:4383.
29. Marezio M, Dernier, PD. Twinning in Cr-doped VO₂. *Acta Cryst.* 1973;A29:618.
30. Goodenough JB. The two components of the crystallographic transition in VO₂. *J. Solid State Chem.* 1971;3:490-500.
31. Strelcov E, Tselev A, Ivanov I, Budai JD, Zhang J, Tischler JZ, Kravchenko I, Kalinin SV, Kolmakov A. Doping-based stabilization of the M2 phase in free-standing VO₂ nanostructures at room temperature. *Nano Lett.* 2012;12:6198-6205.
32. Zhang Y, Jing X, Cheng Y, Hu T, Meng, C. Controlled synthesis of 3D porous VO₂(B) hierarchical spheres with different interiors for energy storage. *Inorg. Chem. Front.* 2018;5:2798-2810.
33. Ndiaye N, Masikhwa T, Ngom B, Madito M, Oyedotun K, Dangbegnon J, Manyala, N. Effect of growth time on solvothermal synthesis of vanadium dioxide for electrochemical supercapacitor application. *Mater. Chem. Phys.* 2018;214:192-200.
34. Ndiaye N, Madito M, Ngom B, Masikhwa T, Mirghni A, Manyala, N. High-performance asymmetric supercapacitor based on vanadium dioxide and carbonized iron-polyaniline electrodes. *AIP Adv.* 2019; 9:1-9.
35. Rakhi RB, Nagaraju DH, Beaujuge P, Alshareef HN. Supercapacitors based on two dimensional VO₂ nanosheet electrodes in organic gel electrolyte. *Electrochim. Acta* 2016;220:601-608.
36. Reddy IN, Sreedhar A, Shim J, Gwag JS. Multifunctional monoclinic VO₂ nanorod thin films for enhanced energy applications: Photoelectrochemical water splitting and supercapacitor. *J. Electroanal. Chem.* 2019;835:40-47.

37. Basu R, Ghosh S, Bera S, Das A, Dhara, S. Phase-pure VO₂ nanoporous structure for binder-free supercapacitor performances. *Sci. Rep.* 2019;9:1-11.
38. Wang J, Zhang X, Zhang Y, Abas A, Zhao X, Yang Z, Su Q, Lan W, Xie E. Lightweight, interconnected VO₂ nanoflowers hydrothermally grown on 3D graphene networks for wide-voltage-window supercapacitors. *RSC Adv.* 2017;7:35558-35564.
39. Ren G, Zhang R, Fan Z. VO₂ nanoparticles on edge oriented graphene foam for high rate lithium ion batteries and supercapacitors. *Appl. Surf. Sci.* 2018;441:466-473.
40. Zhang Y, Zheng J, Hu T, Tian F, Meng C. Synthesis and supercapacitor electrode of VO₂(B)/C core-shell composites with a pseudocapacitance in aqueous solution. *Appl. Surf. Sci.* 2016;371:189-195.
41. Lv W, Yang C, Meng G, Zhao R, Han A, Wang R, Liu J. VO₂(B) nanobelts/reduced graphene oxide composites for high-performance flexible all-solid-state supercapacitors. *Sci. Rep.* 2019; 9:1-8.
42. Lampe-onnerud C, Thomas JO, Hardgrave M, Yde-Andersen S. The performance of single-phase in the lithium/polymer electrolyte battery. *J. Electrochem. Soc.* 1995;142:3648-3651.
43. Lupi S. *et al.* A microscopic view on the Mott transition in chromium-doped V₂O₃. *Nat. Commun.* 2010;1:105.
44. Ding Y. *et al.* Novel high-pressure monoclinic metallic phase of V₂O₃. *Phys. Rev. Lett.* 2014;112:056401.
45. Hou ZQ, Wang ZY, Yang LX, Yang ZG. Nitrogen-doped reduced graphene oxide intertwined with V₂O₃ nanoflakes as self-supported electrodes for flexible all-solid-state supercapacitors. *RSC Adv.* 2017;7:25732-25739.

46. Zheng J, Zhang Y, Meng C, Wang X, Liu C, Bo M, Pei X, Wei Y, Lv T, Cao, G. $\text{V}_2\text{O}_3/\text{C}$ nanocomposites with interface defects for enhanced intercalation pseudocapacitance. *Electrochim. Acta* 2019;318:635-643.
47. Hu T, Liu Y, Zhang Y, Nie Y, Zheng J, Wang Q, Jiang H, Meng, C. Encapsulating V_2O_3 nanorods into carbon core-shell composites with porous structures and large specific surface area for high performance solid-state supercapacitors. *Micropor. Mesopor. Mat.* 2018;262:199-206.
48. Zhang X, Bu Z, Xu R, Xie B, Li, H. V_2O_3 nanofoam@activated carbon composites as electrode materials of supercapacitors. *Funct. Mater. Lett.* 2017;10:1750077.
49. Balog P, Orosel D, Cancarevic Z, Schön, C, Jansen M. V_2O_5 phase diagram revisited at high pressures and high temperatures. *J. Alloys Compd.* 2007;429:87-98.
50. Enjalbert R, Galy J. A refinement of the structure of V_2O_5 . *Acta Cryst.* 1986;C42:1467-1469.
51. Bachmann HG, Ahmed FR, Barnes WH. The crystal structure of vanadium pentoxide. *Z. Kristallogr.* 1961;115:110-131.
52. Yang J, Lan T, Liu J, Song Y, Wei M. Supercapacitor electrode of hollow spherical V_2O_5 with a high pseudocapacitance in aqueous solution. *Electrochim. Acta* 2013;105:489-495.
53. Wee G, Soh H, Cheah Y, Mhaisalkar S, Srinivasan, M. Synthesis and electrochemical properties of electrospun V_2O_5 nanofibers as supercapacitor electrodes. *J. Mater. Chem.* 2010;20:6720-6725.
54. Pandit B, Dubal D, Sankapal B. Large scale flexible solid state symmetric supercapacitor through inexpensive solution processed V_2O_5 complex surface architecture. *Electrochim. Acta* 2017;242:382-389.

55. Liu Z, Zhang H, Yang Q, Chen Y. Graphene/V₂O₅ hybrid electrode for an asymmetric supercapacitor with high energy density in an organic electrolyte. *Electrochim. Acta* 2018;287:149-157.
56. Nagaraju D, Wang Q, Beaujuge P, Alshareef H. Two-dimensional heterostructures of V₂O₅ and reduced graphene oxide as electrodes for high energy density asymmetric supercapacitors. *J. Mater. Chem. A* 2014;2:17146-17152.
57. Choudhury A, Bonso J, Wunch M, Yang K, Ferraris J, Yang D. In-situ synthesis of vanadium pentoxide nanofibre/exfoliated graphene nanohybrid and its supercapacitor applications. *J. Power Sources* 2015;287:283-290
58. Balasubramanian S, Purushothaman K. Carbon coated flowery V₂O₅ nanostructure as novel electrode material for high performance supercapacitors. *Electrochim. Acta* 2015;186:285-291.
59. Chen Z, Augustyn V, Wen J, Zhang Y, Shen M, Dunn B, Lu Y. High-performance supercapacitors based on intertwined CNT/V₂O₅ nanowire nanocomposites. *Adv. Mater.* 2011;23:791-795.
60. Wu Y, Gao G, Yang H, Bi W, Liang X, Zhang Y, Zhang G, Wu G. Controlled synthesis of V₂O₅/MWCNT core/shell hybrid aerogels through a mixed growth and self-assembly methodology for supercapacitors with high capacitance and ultralong cycle life. *J. Mater. Chem. A* 2015;3:15692-15699.
61. Sun W, Gao G, Zhang K, Liu Y, Wu G. Self-assembled 3D N-CNFs/V₂O₅ aerogels with core/shell nanostructures through vacancies control and seeds growth as an outstanding supercapacitor electrode material. *Carbon* 2018;132:667-677.

62. Qian T, Xu N, Zhou J, Yang T, Liu X, Shen X, Liang J, Yan C. Interconnected three-dimensional V₂O₅/polypyrrole network nanostructures for high performance solid-state supercapacitors. *J. Mater. Chem. A* 2015;3:488-493.
63. Bi W, Huang J, Wang M, Jahrman E, Seidler G, Wang J, Wu Y, Gao G, Wu G, Cao, G. V₂O₅-conductive polymer nanocables with built-in local electric field derived from interfacial oxygen vacancies for high energy density supercapacitors. *J. Mater. Chem. A* 2019;7:17966-17973.
64. Xu J, Zheng F, Xi C, Yu Y, Chen L, Yang W, Hu P, Zhen Q, Bashir S. Facile preparation of hierarchical vanadium pentoxide (V₂O₅)/titanium dioxide (TiO₂) heterojunction composite nano-arrays for high performance supercapacitor. *J. Power Sources*. 2018;404:47-55.
65. Nie G, Lu X, Lei J, Jiang Z, Wang C. Electrospun V₂O₅-doped α -Fe₂O₃ composite nanotubes with tunable ferromagnetism for high-performance supercapacitor electrodes. *J. Mater. Chem. A* 2014;2:15495-15501.
66. Jayalakshmi M, Rao M, Venugopal N, Kim K. Hydrothermal synthesis of SnO₂-V₂O₅ mixed oxide and electrochemical screening of carbon nano-tubes (CNT), V₂O₅, V₂O₅-CNT, and SnO₂-V₂O₅-CNT electrodes for supercapacitor applications. *J. Power Sources* 2007;166:578-583.
67. Kiruthiga R, Nithya C, Karvembu R. Reduced graphene oxide embedded V₂O₅ nanorods and porous honey carbon as high performance electrodes for hybrid sodium-ion supercapacitors. *Electrochim. Acta* 2017;256:221-231.
68. Liu K, Lee S, Yang S, Delaire O, Wu J. Recent progresses on physics and applications of vanadium dioxide. *Mater. Today* 2018;21:875-896.

69. Huang H, Song Y, Liu XX. Boosting operating voltage of vanadium oxide-based symmetric aqueous supercapacitor to 2 V. *Chem. Eng. J* 2019;358:1529-1538
70. Zhao D, Zhu Q, Chen D, Li X, Yu Y, Huang X. Nest-like V_3O_7 self-assembled by porous nanowires as an anode supercapacitor material and its performance optimization through bonding with N-doped carbon. *J. Mater. Chem. A* 2018;6:16475-16484.
71. Toriyama T, Nakayama T, Konishi T, Ohta Y. Charge and orbital orderings associated with metal-insulator transition in V_6O_{13} . *Phys. Rev. B* 2014;90:085131.
72. Zhai T, Lu X, Ling Y, Yu M, Wang G, Liu T, Liang C, Tong Y, Li Y. A New benchmark capacitance for supercapacitor anodes by mixed-valence sulfur-doped V_6O_{13-x} . *Adv. Mater.* 2014;26:5869-5875.
73. Pang HC, Dong YQ, Ting SL, Lu JL, Li CM, Kim DH, Chen P. 2D single- or double-layered vanadium oxide nanosheet assembled 3D microflowers: Controlled synthesis, growth mechanism, and applications. *Nanoscale* 2013;5:7790.